Structural collapse in phlogopite mica-rich mine tailings induced by mechanochemical treatment and implications to alkali activation potential

He Niu, Paivo Kinnunen*, Harisankar Sreenivasan, Elijah Adesanya, Mirja Illikainen

Fibre and Particle Engineering Research Unit, University of Oulu, P.O. Box 4300, FI-90570, Oulu, Finland

A B S T R A C T

The alkali activation of mine tailings is of interest to diminish the impoundment storage of large waste stream from mining industry. However, most of the mine tailings, like phosphate mine tailings generated in Finland, are rather inert and need pre-treatment to induce the reactivity for alkali activation. In this work, mechanochemical treatment was conducted to improve the reactivity of phosphate mine tailings. The ground specimens were subjected to the crystal structural analysis of X-Ray diffraction (XRD), X-ray photoelectron spectroscopy (XPS), and thermal analyses by Thermogravimetry/Differential Thermal Analysis (TG/DTA), showing the increment of amorphous content and structural degradation as a function of grinding time. The subsequent alkaline reactivity test illustrated incremental alkaline dissolution of Si, Al and K and a schematic diagram of altered phlogopite structure (sources of aluminosilicates in tailings) was also proposed. Additionally, the mineralogical composition of individual particles was carried out by mineral liberation analysis (MLA), thereby evaluating the influence of pre-treatment on the mineralogy of tailings. The results indicate profound micromorphological changes and structural cleavage of the precursor due to grinding, which strongly increase alkaline reactivity.

1. Introduction

In recent years, the frequency of extreme climates has considerably increased due to excessive emission of carbon dioxide generated from human activities. One of the biggest source of carbon dioxide emissions is the manufacturing of cement and concrete, which has become the second largest commodity across the world except for only water (Aïtcin, 2000). The traditional production of Ordinary Portland Cement (OPC) involves the calcination of raw meals at about 1,400–1,450 °C (Vatopoulos and Tzimas, 2012). Furthermore, the cement industry totally emits around 0.9 tonnes of carbon dioxide for producing each tonne of Portland cement (Hasanbeigi et al., 2010).

Alkali-activated materials (AAMs) have become widely studied in the application of construction due to their sustainability and low CO_2 emission (Turner and Collins, 2013). Moreover, AAMs have shown benefits in several aspects over OPC like mechanical properties (Duxson et al., 2007), fire resistance (Cheng and Chiu, 2003; Vickers et al., 2015), acid resistance (Xu and Van Deventer, 2000), heavy metal stabilization and flexible curing time (Sarker et al., 2014; Ye et al., 2016). Alkali activation is a method to produce cementitious binders which are classified into two systems: high-calcium AAMs and low-calcium AAMs (geopolymers) (J. Provis, 2014). The high-calcium system generates C-

(N-)A-S-H[1] type gel with a moderate alkaline solution, while its low-calcium counterpart produces N-A-S-H type gels after alkali activation by medium or high alkaline solutions (J.L. Provis, 2014). Additionally, AAMs can be produced from industrial waste or natural minerals, which has desirable chemical reactivity for alkali activation. Those glassy precursors such as blast furnace slag (Douglas et al., 1991), fly ash (Phair and van Deventer, 2002), other pozzolanic minerals (Xu and Van Deventer, 2000) show highest potential, while mine tailings rich in aluminosilicate or carbonate minerals are less investigated (Kinnunen et al., 2018).

Mine tailings are usually stored near the mining sites in tailings ponds (Ávila et al., 2008). Although mining wastes have been used in alkali activation, the utilization of precursors is difficult due to the poor reactivity. Consequently, to further investigate various minerals and elucidate the internal correlation behind such complex industrial residues is of vital importance. Moreover, pre-treatment is essential before alkali activation for mine tailings, in which different methods have been conducted such as blending (Choi and Lee, 2012, p. 3; Giannopoulou and Panias, 2006; Jiao et al., 2013; Kiventerä et al., 2016; Moukannaa et al., 2018; Song et al., 2016; Van et al., 2000), calcination (Fernando et al., 2010; Pacheco-Torgal et al., 2009; Silva et al., 2012; Ye et al., 2014), and ball milling (Kalinkina et al., 2018;

---

* Corresponding author.
  E-mail address: Paivo.Kinnunen@oulu.fi (P. Kinnunen).
[1] C-CaO, N-Na₂O, A-Al₂O₃, S-SiO₂, H-H₂O.

Wei et al., 2017).

The vibratory disc mill, one of mechanochemical technologies, induces plastic deformation and internal stress resulting in higher kinetic energy than attrition mill (ball mill) (Kumar et al., 2007), during which materials experience the transformation from crystalline to amorphous phase through a metastable state. At the same time, it also promotes chemical reactions at particle surfaces induced by sudden impact between particles or grinding media, producing high surface energy and large specific surface area (Plescia et al., 2003). Aglietti et al. (1986) carried out the mechanical activation of kaolinite, of which amorphization and incremental surface energy gave rise to improved chemical reactivity. Mechanochemically activated fly ash was subjected to alkali activation, achieving a high compressive strength of 45 MPa after 8-day curing under ambient condition (Temuujin et al., 2009). Mechanochemical technology also showed some advantage as a pre-treatment method on 2:1 layer lattice phyllosilicates (MacKenzie et al., 2008). The thermal behaviours of talc after mechanical activation was investigated (Liao and Senna, 1992), illustrating the transformation of amorphized talc into enstatite caused by structural destruction and dehydroxylation. As for phosphate mine tailings (phyllosilicates-bearing tailings); however, little is known on the effect of mechanochemical treatment. It is necessary to explore their potential in alkali activation and the mechanism of mechanochemical treatment. The aim of this work, therefore, is to study the effect of grinding on phosphate mining wastes and the potential of ground tailings as alkali activation precursors. In addition, MLA was used to illustrate the mineralogical alternation after mechanochemical activation, which aims to obtain in-depth understanding of mineral interaction within individual particles. This technology has not been implemented in the assessment of geopolymer precursors so far, although it is widely used in minerals engineering like comminution (Ozcan and Benzer, 2013; Vizcarra et al., 2010; Xiao et al., 2012).

2. Materials and methods

The phosphate mine tailings (PMT) was obtained from Siilinjärvi phosphate mining site (Yearly production:10 Mt/a; Stock: 280 Mt), Finland, which mainly consist of phlogopite (64%), dolomite (6%), calcite (14%) and tremolite (1.4%). The mineralogy of mining site is carbonatite and apatite-bearing rocks with in-situ grade of 4.2% P_2O_5. It should be noted that the PMT was received as coarse and granular materials. The chemical composition of PMT was identified by a PANalytical AXios^{mAX} XRF spectrometer with a rhodium tube which has a maximum power rate of 4 kW (Table 1). Deionized water was used throughout the work.

Vibratory disc mill (Retsch RS 200) was used for mechanochemical activation. The pristine PMT was ground for periods of 1 min, 2 min, 4 min, 8 min, and 16 min at 1,500 rpm with 0.5 wt% grinding aid (2-propanol; $\geq$ 99.7%; VWR Chemicals), and the samples were dubbed (Gt, where t specifies the grinding time in minutes). Particle size distribution (PSD) was determined by a laser diffraction particle size analyser (LS 13320, Beckman Coulter, Inc., Brea, CA, USA). Specific surface area was measured by ASAP 2000 Micrometrics based on Brunauer–Emmett–Teller (BET) theory, which means the physical adsorption of nitrogen molecules on solid surface. XRD analysis of ground samples was subjected to a Rigaku SmartLab 4.5 kW, with the equipment parameters of Co source (40 kV and 135 mA) K_α ($K_{\alpha 1}$ = 1.78892 Å; $K_{\alpha 2}$ = 1.79278 Å; $K_{\alpha 1}$ /$K_{\alpha 2}$ = 0.5), scan rate of 3°/min and 0.02°/step. Quantitative analysis was performed by using

PDXL2 Software Suite with integrated access to PDF-4 (2019) database. 10 wt% Rutile (powder; < 5 μm; ≥99.9% trace; metal basis) was used as internal standard, homogenized with ground PMT by using an agate mortar. In addition, ground powder was subjected to thermal analysis by Netzsch STA 449 F3 TGA-DTA/DSC analyser (Selb, Germany) with Mass spectrometry (MS) to record released water and carbon dioxide molecules. Specimen, about 20 mg, was placed in a platinum crucible with lid, kept in the furnace to 1,550 °C with a heating rate of 10 °C/min under the inert atmosphere. X-ray photoelectron spectroscopy (XPS) analysis was conducted by using Thermo Fisher Scientific ESCALAB 250Xi XPS System. The binding energy adventitious carbon (C_{1s} = 284.8 eV) was used for the calibration. The samples were placed on an Indium membrane with passing energy of 20 eV and spot size of 900 μm. Elements which induces Si, Al, O, K, Mg and Ca were measured in all specimens. All the ground samples (including phosphate mine tailings) are subjected to alkaline reactivity evaluation by mixing with 6 M NaOH solution in polypropylene bottles at a liquid/solid mass ratio of 200/1. A horizontal shaking table (IKA KS 260 orbital shaker) was utilized at Mot = 150/min for 24 h, during which a moderate environment was set at 23 $\pm$ 0.5 °C. Thereafter, the resulting specimens were filtered by using a 0.2 μm filter paper and the filtrate was acidified by 6 M HNO_3 to pH lower than 1. The dissolved fraction of Si, Al, Mg, Fe, Ca and K elements was measured by the inductively coupled plasma-optical emission spectroscopy (ICP-OES) technique. BSE images were collected via a Scanning Electron Microscopy (SEM) with Energy-dispersion spectroscopy (EDS) and Mineral Liberation Analysis was performed on 1-min and 16-min samples to evaluate the mineralogical change within each particle. Once the particles were isolated (milled with graphite), the individual mineral was outlined with its unique average atomic number (AAN) which shows as grey level, of which AAN identifies the number of backscatter electrons emitted from the mineral (Fandrich et al., 2007).

The alkali activator was prepared by adding sodium hydroxide pellets into sodium silicate solution to make M_s = 2 (that is, SiO_2/Na_2O = 2). The alkali-activated mine tailings were synthesized by addition 100 g mine tailings (Raw PMT, G2, and G16) to 90 g alkali activator with solid/liquid ratio of 2. The paste was moulded in plastic cylindrical mould with 20 mm height and 25 mm diameter, followed by curing at 40 °C sealed in the plastic bag. The hardened sample was demoulded and cured until 7 days under sealed condition at room temperature. The unconfined compressive strength (UCS) was performed with the Zwick 10 kN machine with a loading force of 2.4 kN/s until failure.

3. Results and discussion

3.1. Particle size distribution (PSD) and BET surface measurement

The grinding has an explicit effect on the particle size distribution and specific surface area. Particle size reduces linearly until 4-min grinding, after which no big change is observed (Fig. 1).

The specific surface area as measured by BET method considerably increases from 0.1604 m^2/g (G0) to 13.9362 m^2/g after 16-min grinding of raw tailings. The specific surface area increases monotonously with grinding time, while D50 is not consistent showing signs of agglomeration between 8 and 16 min of grinding. Presumably primary particles continue to be ground smaller, increasing internal porosity of the agglomerates (Marjanović et al., 2014). No change in particle size distribution is observed between 4 and 16 min of grinding

Table 1
XRF analysis of PMT (% w/w) (LOI: loss on ignition).

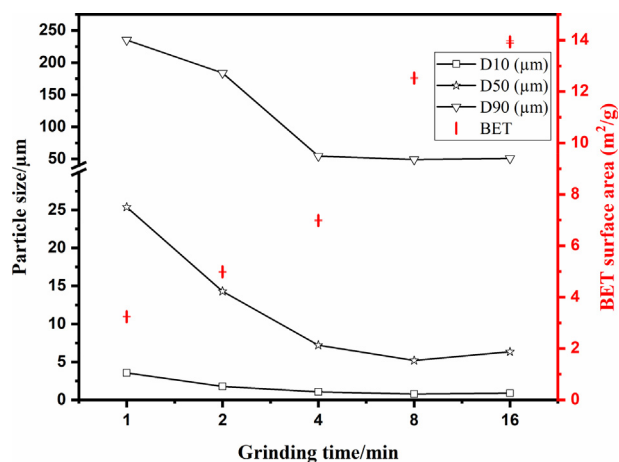| Components	SiO_2	Al_2O_3	CaO	MgO	K_2O	Fe_2O_3	P_2O_5	TiO_2	MnO	Others	L.O.I.
Weight %	32.99	7.09	12.92	17.27	5.53	7.99	0.95	0.27	0.12	0.86	14.01

Fig. 1. Particle size distribution and BET surface area of ground samples.

Fig. 3. Reflection (h k l) changes in X-ray diffraction diagrams of ground samples.

even though the crystalline structure is considerably disrupted as seen by XRD.

3.2. XRD analysis

As observed by XRD (Fig. 2), the main components are calcite (ICDD, PDF-4 #04-012-0489), dolomite (ICDD, PDF-4 #04-015-9848), phlogopite (ICDD, PDF-4 #04-012-5381), tremolite (ICDD, PDF-4 #04-013-2249). In addition, 10 wt% rutile (ICDD, PDF-4 #04-007-4874) was added as an Internal standard. It should be mentioned that the vertical axis of XRD patterns shows in logarithmic scale, which favours the conspicuous expression of peak alternation (Terashima et al., 2006).

The diffractograms show line broadening from G1 through G16 among all the components because of the structural degradation by vibratory disc mill (Kristof and Juhasz, 1993). The increasing collapse of the structure resulted from plastic deformation produced by two actions of shear force and friction between particles and grinding media (Martinelli and Plescia, 2004, p. 2). Calcite and dolomite, category of carbonate minerals, experienced the structural changes during the mechanochemical treatment. After 16-min grinding, only some peaks of calcite still exist with broad band, which coincides with that grinding can cause more noticeable change in the peak area than peak height (Gavish and Friedman, 1973). Dolomite peaks cannot be recognized from the background and it is practically amorphous after 16-min grinding. The continuous transformation of calcite-aragonite is not observed in this work possibly due to the noisy background of sophisticated mineral complex (Criado and Trillo, 1975).
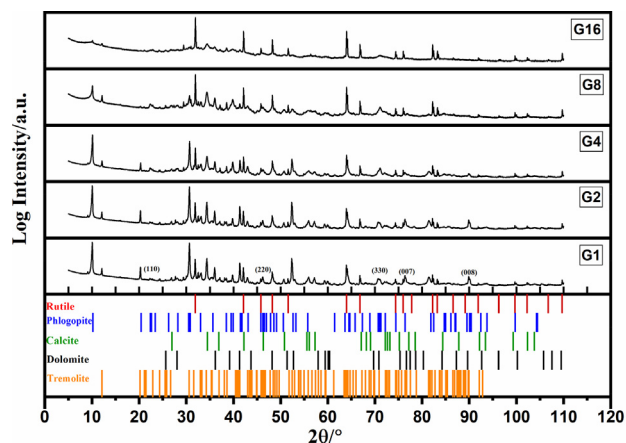

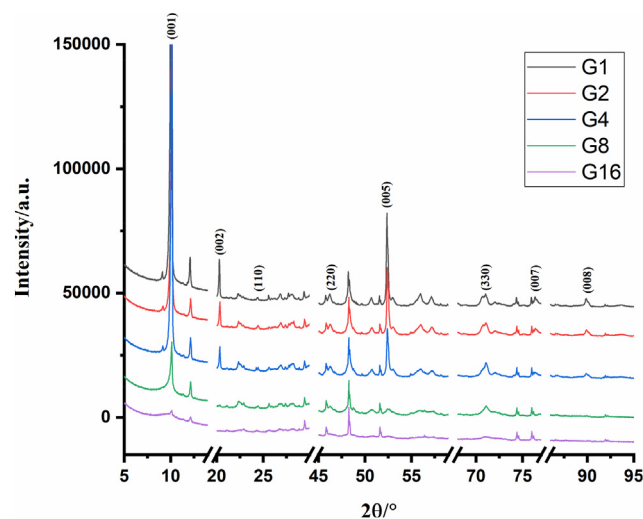**Fig. 2.** XRD profiles of PMT ground with different grinding time. (Internal standard as rutile).

The grinding clearly affected the structure of phlogopite. Phlogopite is one of the 2:1-layer lattice aluminosilicates, where Mg octahedral sheet is sandwiched between two Si, Al tetrahedral layers (T-O-T structure) with K^+ ions filling in the interlayer (general 2:1-layer lattice aluminosilicate structure (Rayner, 1974)). The peak intensity considerably reduces from G8 to G16, in which few peaks of phlogopite can be distinguished from the background. In addition, the decrease of tremolite peak intensity was reported in the literature stated that tremolite lost crystallinity after 10-min grinding (Bloise et al., 2018b).

Phlogopite layer structure was seen to almost completely collapse during extended mechanochemical treatment. Cleavage along c-axis is indicated by the disappearance of the phlogopite (0 0 l) reflections. The position of the highest (0 0 1) X-ray diffraction peaks reflects the interplanar distance, d, which is the fundamental repeating distance in the perpendicularly stacking 2:1-layer structure (Bigham et al., 2001). This phenomenon is in accordance with the results of ground layer aluminosilicates such as pyrophyllite (Sanchez-Soto et al., 1994). In addition to the dramatic drop in peak intensity, the position of the peak changed as well. The (0 0 1) peak position has the trend to shift to a higher angle with the incremental milling time (Fig. 3). This phenomenon can be explained by the change of lattice strain and the increase in lattice defects during grinding.

The d value shows a small drop between G1 and G2, which is possibly due to the attractive electrostatic interaction between interlayers. The general (h k l) reflections including (1 1 0), (2 2 0) and (3 3 0) are also highly altered but change less dramatically (Fig. 3).

The XRD patterns of ground samples with internal standard were subjected to quantitative analysis by using WPPF method (Whole Powder Pattern Fitting). Most crystalline phases in mine tailings transferred to amorphous counterparts after 16-min grinding, in which the amount of phlogopite obtained the significant change (Fig. 4a). The overall incremental amorphous content (%) with function of residence time is presented in Fig. 4b. The amorphous content reached the value of more than 70% after 16-min grinding.

3.3. Thermal analyses

16-min grinding considerably affected tailings' thermal behaviour, indicating extensive structural alternation. The samples G1 through G8 provide the analogous trend on both TGA and DTA curves, while G16 presents explicitly different thermal behaviours during the thermal measurement (Fig. 5a, b). As for sample G1 to G8, the endothermic peak centred at 700 °C is associated with the release of carbon dioxide; that is, the decomposition of dolomite ($MgCa(CO_3)_2$) and calcite
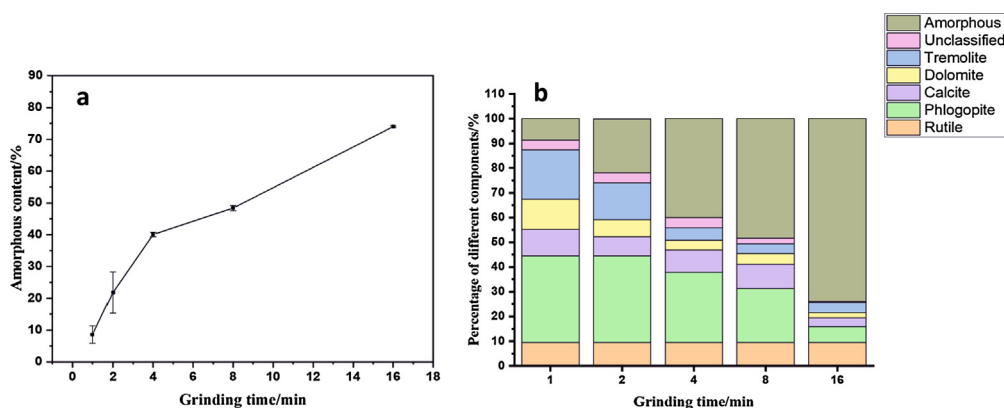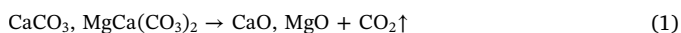
Fig. 4. (a) Quantitative phase analysis of PMT with different milling time, (b) amorphous content change with variation of grinding time.

according to the reaction Eq. (1) (Földvári, 2011).

$$CaCO_3, MgCa(CO_3)_2 \rightarrow CaO, MgO + CO_2\uparrow \qquad (1)$$

Since the tiny sample mass of 20 mg and structural similarity of both carbonates, the thermogram exclusively expresses a large peak representing small CO_2 partial pressure for a combined reaction above-mentioned (Kristóf-Makó and Juhász, 1999; WARNE, 1977). From 900 °C to 1,100 °C, the structure of phlogopite disrupted in accordance with a progressive dehydroxylation, and the tremolite decomposed into pyroxene, silica and water (Bloise et al., 2018b; Tutti et al., 2000), which coincides with a hump on the water (H_3O^+) trace and is also in line with the research of Tutti et al. (2000) (Fig. 5c). A broad

endothermic peak at 1,200 °C appears in the DTA curve of G1, which demonstrates that the sample was gradually decomposed; that is, the breakage of oxygen-bridge bond. This process becomes less apparent in G2, thereafter, it completely converts to an exotherm when the milling time increases to post-4 min. It also happened in similar studies on 2:1-layer lattice minerals such as pyrophyllite (Fandrich et al., 2007; Marjanović et al., 2014; Ozcan and Benzer, 2013). Another investigation on talc, also a 2:1-layer lattice mineral, indicated that the excess energy from grinding was stored in the Al-Si tetrahedra layer, which preferentially broke Al-O and Si-O bonds then became Al-Si amorphous phases (Liao and Senna, 1992). Therefore, the researchers hypothesized that the appearance of the exothermic peak at 1,200 °C was the
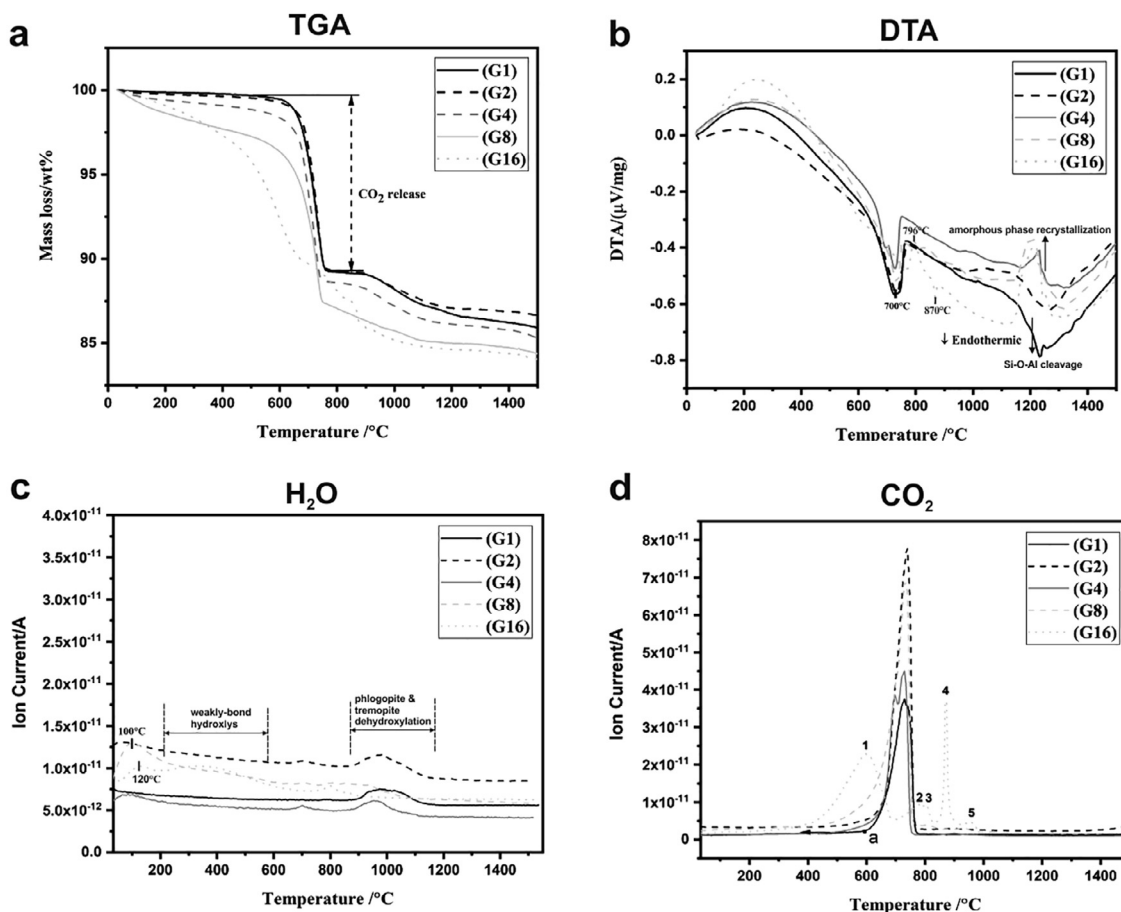

Fig. 5. Thermal analysis of ground samples, (a) TGA analyses, (b) DTA analyses, (c) Mass spectroscopy (MS) of water and (d) Mass spectroscopy (MS) of carbon dioxide.
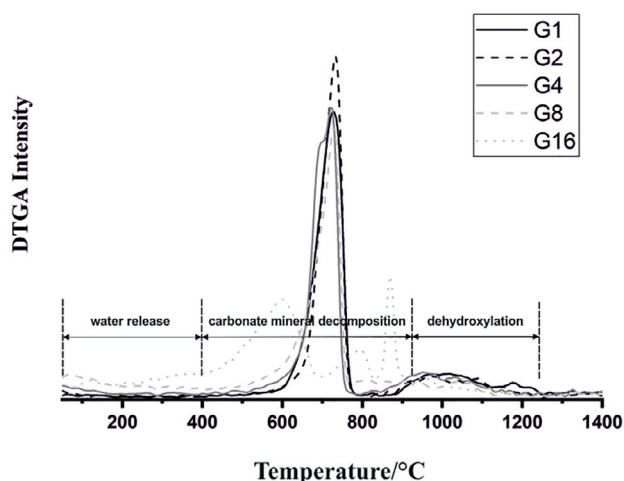
Fig. 6. DTGA intensity spectra of ground specimens.

evidence of Si-O-Al linkages in non-crystalline aluminosilicates (re)crystalizing to such as mullite (Terashima et al., 2006). Additionally, the increase of free oxygen (O^{2-}) during mechanochemical treatment enhanced this crystallization. In other words, amorphous or semi-crystalline phases with high surface energy started to crystallize during heating, presenting an exothermic behaviour.

The thermal features of G16 are completely different from the others because of its high amorphous content. From a general point, the structure of raw materials experienced obvious changes from crystalline to amorphous phase. Moreover, it reflects the improved chemical reactivity by bond cleavage arising from mechanochemical activation. Surface water and interlayer water removal become more obvious below 400 °C when compared with G1 and G2; it is consistent with the interpretation that a bulk of weakly bonded hydroxyls appeared at around 350 °C after 16-min grinding (Fig. 5c). It is reasonable to assume that the hump at about 120 °C on water trace results from the water release in the transformation between calcite and aragonite, which can be found in other studies about mechanically treated calcite (Burns and Bredig, 1956; Földvári, 2011). Furthermore, the H^+ from proton migration during the intense grinding reacted with OH^- groups, forming more water molecules as shown in Eq. (2) and Eq. (3) (Bloise et al., 2018a). Another evidence is that the disappearance of OH^- peak at around 1,000 °C on G8 and G16 compared with that of G1 to G4, showing that most of hydroxyls reacted during mechanochemical treatment.

$$OH^- \rightarrow H^+ + O^{2-} \tag{2}$$

$$H^+ + OH^- \rightarrow H_2O \tag{3}$$

The onset temperature of CO_2 release (point **a** in Fig. 5d) shifts to a lower temperature in CO_2 MS-curve due to the storage of extra surface energy in amorphous phases, thereby reducing the activation energy (Fig. 5d) (Liao and Senna, 1992). A distinct double peak (dolomite; 670 °C) appears in the MS curve of CO_2 in G4, which elucidates the separate decomposition of dolomite and calcite. The summit decreases from 730 °C to 712 °C and 702 °C corresponding to from G1 to G2, and G4 respectively. It means that the grinding increases the magnitude of lower temperature endothermic reaction at the expense of higher temperature endothermic reaction within dolomite (Bradley et al., 1953). There are five peaks representing different carbon dioxide release in the curve of G16 (Fig. 5d), of which the peak 1 at 579 °C is associated with the decomposition of Type-II $MgCO_3$ (disordered dolomite) layer; that is, amorphous carbonate minerals at a lower temperatures from 400 °C to 700 °C (Kristof and Juhasz, 1993). The appearance of $MgCO_3$ (MgII) results from the degradation of dolomite after a prolonged grinding time (Kristóf-Makó and Juhász, 1999). The

peak 2 at 783 °C is ascribed to Type-I $MgCO_3$ (crystalline dolomite), followed by the decomposition of amorphous $CaCO_3$ (peak 3; 802 °C). At the meanwhile, the oxidation of Fe^{2+} (796 °C, Eq. (5); Fig. 5b) occurs overlapping with the decomposition of $CaCO_3$ at around 800 °C (Földvári, 2011); it is also induced by amorphization of clay minerals, accelerating the mobility of ions.

$$MgCa(CO_3)_2 \rightarrow CaCO_3 + MgO + CO_2\uparrow \tag{4}$$

$$2Fe^{2+} + 2OH^- \rightarrow 2Fe^{3+} + 2O^{2-} + H_2\uparrow \tag{5}$$
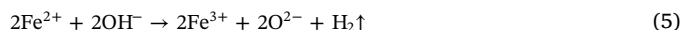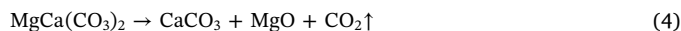
It is unlike with the dehydroxylation of non-iron-bearing 2:1-layer lattice silicates such as pyrophyllite and muscovite (Udagawa et al., 1974; Wardle and Brindley, 1972), where the residue oxygen from Eq. (2) moves to Al cation. When the dehydroxylation was conducted by mechanochemical treatment, the O^{2-} showed a propensity to react with ferrous ions in phlogopite. It is also in accordance with the results of Fe-contained pyrophyllite studied by Heller-Kallai and Rozenson, in which all the iron became trivalent form after thermal dehydroxylation (Heller-Kallai, 1980). The peak 4 corresponds with a sharp carbon dioxide emission from the calcite obtained from Eq. (4), located at 870 °C (Kristof and Juhasz, 1993). The peak 5 is well agreed with the decomposition of well-crystalline $CaCO_3$ residue at 956 °C in the literature (Liao and Senna, 1992).

In order to get a scope into mass change in different ranges of temperature, the TGA data was differentiated to derivative-TGA (DTGA) spectra and smoothed via Adjacent-Averaging method as shown in Fig. 6. The total mass loss is given in Table 3. The initial mass loss starts from a lower temperature with extended milling time. The DTGA traces (G1 to G4) present three major weight-loss stages: 1) 50 °C to 400 °C arose from the removal of physically adsorbed water and crystal water, 2) 500 °C to 800 °C, decomposition of dolomite and calcite, 3) 900 °C to 1,300 °C, resulted from the dehydroxylation of phlogopite and tremolite (Bloise et al., 2018b; Sreenivasan et al., 2017a). This phenomenon is agreed with that tremolite and phlogopite are all thermally stable before 900 °C. A continuous mass loss after 900 °C reflects the collapsed sample structure, corresponding to the endothermic peak in the DTA graphs of G1 and G2 (Fig. 5b). It should be mentioned that the vague boundary appears between 2nd and 3rd stage in G8 curve due to the increasing amount of disordered dolomite (MgII) and calcite during mechanochemical activation. Whilst the G16 shows a different course of decomposition with the formation of Si-O-Al linkages, accompanied with the high temperature dehydroxylation. The DTGA curve of G16 resembles its CO_2 release trace, which means that the release of CO_2 has more pronounced effect than that of hydroxyl on weight loss since the majority of dehydroxylation was achieved during grinding rather than thermal analysis and the discrepancy of molar mass between CO_2 and H_2O.

3.4. XPS analysis and alkaline reactivity

XPS analysis is a convenient method for understanding the chemical state of the elements on the surface of solid matters (Siegbahn and Nordling, 1967). It can be used to determine the binding energy of various elements, which is related to the electronic environment of the concerned element (Nefedov, 1988). Here XPS analysis is used to understand the changes happening in the sample because of excessive grinding process. Consistent with the XRD findings, tetrahedral phlogopite layer remains intact, while Mg octahedral layer encountered chemical shifts during the grinding. The binding energies of silicon and aluminum are practically unaffected by grinding (Fig. 7). Silicon and aluminum form the tetrahedral layer of phlogopite. Magnesium binding energy shows shift to lower energies with elevated grinding time. Magnesium is present in two forms in the sample: (1) Magnesium forming octahedral layer of phlogopite; (2) Magnesium forming dolomite. Dolomite decomposition (which involves transformation of $MgCO_3$ to MgO) is evident in the XRD analysis and thermal analyses.
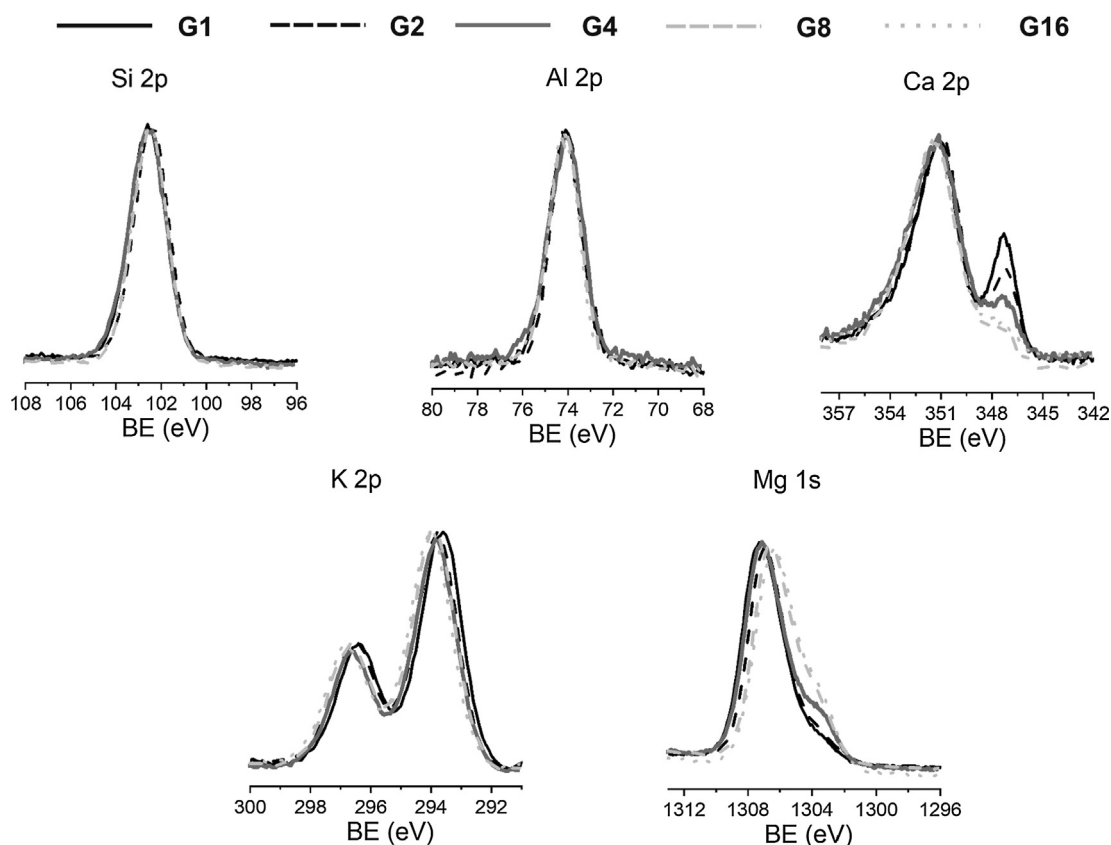
Fig. 7. Results of the XPS analysis for ground samples.

This chemical transformation is reflected in the magnesium binding energy (Changes in chemical state of magnesium forming octahedral layer of phlogopite is ruled out as this agrees with observations made in case of silicon, aluminum binding energies). Binding energy of calcium shows changes due to grinding. This change agrees with the previous XRD observations about the decomposition of dolomite as well as the reduction in intensity and the peak broadening of calcite component. The binding energy of potassium shows slight shift towards higher binding energy due to mechanochemical treatment, which reveals changes in chemical bonding of potassium occupying the interlayer of phlogopite structure.

The alkaline reactivity test reveals original PMT is poorly reactive in alkali activation, whilst its reactivity is considerably increased after mechanochemical activation. Thus, the dissolved fraction of each elements is given as a function of grinding time (Fig. 8). It emphasizes how mechanochemical treatment impacts the alkaline reactive. The concentration of potassium ion demonstrates a surge after only 1-min grinding compared with the tendency of other elements. The sudden increase of K^+ arises from the alkali cation exchange between K^+ in the interlayer and smaller Na^+ in the sodium hydroxide solution during the alkaline reactivity test. It can be observed that Si dissolution shows significant elevation with extended grinding time, achieving more than 25-fold growth after 16-min grinding. Furthermore, the amount of Si dissolution is larger than that of Al since the inherent element content of Al (4%) is rather lower than that of Si (17%) in raw tailings. The Si and Al dissolution of G16 achieve 9.1% and 4.9% with corresponding absolute value of 441.9 mg/L and 57.4 mg/L, respectively. The concentration of Mg and Fe remains steady at about 0 wt% without correlation on grinding time, since both elements are expected to precipitate when dissolved in sodium hydroxide solution consistent with previous research (Sreenivasan et al., 2017b). In general, mechanochemical treatment is promising to improve the chemical reactivity of PMT.
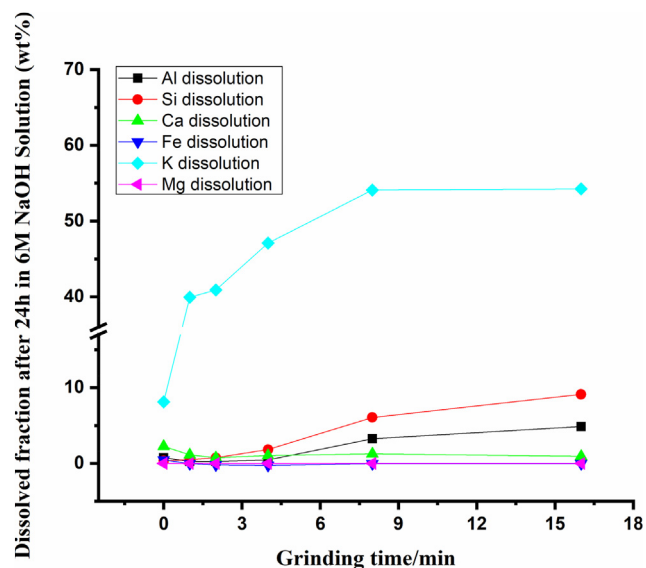

Fig. 8. Alkaline reactivity as a function of grinding durations (0 min means pristine PMT).

3.5. Changes phlogopite mineral structure during grinding

Due to the major component of phlogopite in tailings, the discussion here will focus on its structural alternation during mechanochemical activation. The chemical bonds in phlogopite can be classified as ionic bond between OH and Mg in the octahedral layer and partly covalent bond (or ionic bond) between O and H, covalent bond as Si-O, Al-O in the tetrahedral layer and van der Waals bond (electrostatic force) between the interlayers (Fig. 9). After a short time grinding (1 to 8 min),
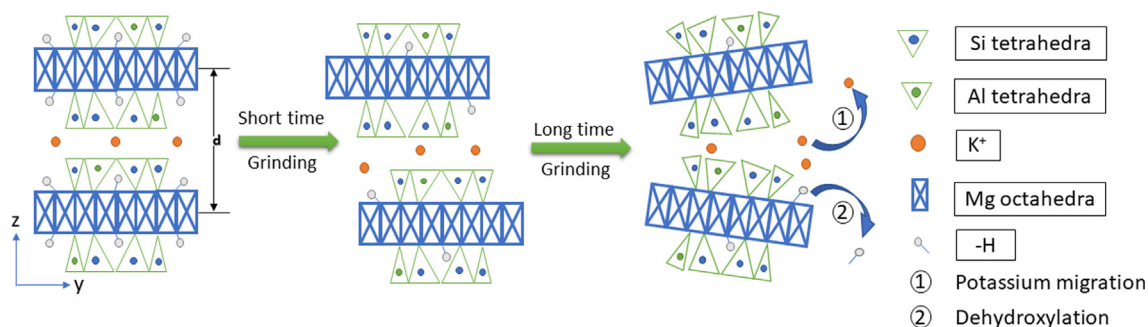
Fig. 9. Schematic diagram of phlogopite structure change during grinding.

Table 2
Change of reflection (0 0 1) for phlogopite.

Sample name	2 theta/(deg)	d/(ang.)
G1	10.091	10.169
G2	10.064	10.197
G4	10.121	10.140
G8	10.123	10.138
G16	10.061	10.201

Table 3
Weight loss of ground samples.

Name	Total mass loss (%)
G1	14.29
G2	13.43
G4	14.82
G8	15.75
G16	16.14

the shear force and impact lead to the dislocation of T-O-T layer with adjacent one, where the interlayer cations play the role like lubricant. It should be noted that the interlayer distance (d) changed less during this process (Table 2). Therefore, it is reasonable to assume that the interlayer dislocation occurred within a short-time grinding, while the interlayer structural practically collapsed after a long-time grinding (16 min). This assumption can be verified by the preceding XRD analysis, XPS analysis and alkaline reactivity test (Fig. 2, Fig. 7, and Fig. 8). The adjacent T-O-T layers dislocate, therefore, K^+ dissolution profoundly increases after a short-time grinding. Additionally, the growth of Si and Al dissolution also reflects the interlayer degradation, for sodium hydroxide solution can attack more internal tetrahedral units after 16-min grinding. The dehydroxylation occurs partially within the octahedral layers, which is associated with the gradual disappearance of the peak on water traces at 900 to 1,000 °C (Fig. 5c). Nevertheless, the structure of phlogopite is not completely disrupted because of the extremely stable Si-O and Al-O bonds, which is also reflected by the unaffected Al and Si bonding energies in XPS analysis. Consequently, this analysis explains amorphization taking place under the following sequence: 1) interlayer disruption, 2) dehydroxylation of the ionic Mg-OH bond, 3) disruption of the aluminosilicate tetrahedra. This structural change is found to be analogous with mechanically treated trioctahedral 2:1-layer silicates talc (Liao and Senna, 1992).

3.6. Morphology and mineralogy analysis

The acquisition of BSE images was based on the MLA, which is basically used to identify mineralogical components of individual particles. BSE images reveal that particles can be classified as three major mineral groups based on grey level, namely, phlogopite, calcite and dolomite (Fig. 10c), which agrees with the results of the XRD analysis.

The particle morphology of G1 shows regular shaped particles, while G16 possesses irregular shaped grains (Fig. 10a, b).

As for sample G1, it shows that most of particles solely contain one mineral except a few large grains or interlocked particles. The particle morphology contains needle-like grains and plate-like grains under 2-dimentional images with stereological bias to some extent. Compared with G1, there are few acicular particles presenting in sample G16 and most grains show irregular shape. It means that the cleavage of acicular particles happens during mechanochemical activation, generating smaller platelike grains or irregular fragments. In addition, small grains are found to aggregate to particles as large as 500 μm consisting of different minerals, generally agreeing with the conclusion drawn from PSD and specific surface area analyses. The increment of irregular particles in G16 demonstrates the generation of amorphous phase, which is in line with the result of XRD analysis. It should be noted that the inherent limitation of MLA system can lead to partial loss of information about 1–2 μm sized particles (Sutherland and Gottlieb, 1991). In terms of PSD, it shows that about 10% particles have the grain size lower than 1 μm. The mineralogical composition of one particle is shown, in which phlogopite is the main component and interlocks with dolomite enclosing an actinolite entity. It implies that these minerals can interact with each other during grinding. This phenomenon may result from the defective phlogopite allowing other smaller crystals connected. The mineral distribution is inhomogeneous within individual particles and larger BET surface area is obtained, furthermore, alkaline reactivity test suggests that it can favour the reaction with alkali activators in the subsequent activation. Therefore, it is reasonable to state that mechanochemical treatment can improve the reactivity of the tailing precursor.

3.7. Alkali-activated mine tailings-preliminary test

The alkali-activated mine tailings paste displayed high relevance with the reactivity of precursors (Fig. 11). The raw mine tailing is not suitable for alkali activation since it did not set after curing under the current experimental conditions. As for AAMs generated by G2, the paste sets and demoulded 24 h. However, it is not hardened sample after 7 day curing which is too soft to conduct compressive strength test. On the contrary, AAMs produced by G16 exhibited relatively good performance as compressive strength reached 4 MPa after 7 days of sealed curing. It revealed that the mechanochemical activation can profoundly alter the reactivity of mine tailings, by which it increased the degree of amorphization as shown by the abovementioned results such as XRD analysis. The future research will be continued on the alkali activation process and the application of mine tailings via alkali activation.

4. Conclusion

This work shed the light on the mechanochemical treatment of phosphate mine tailings as a precursor for alkali activation, which
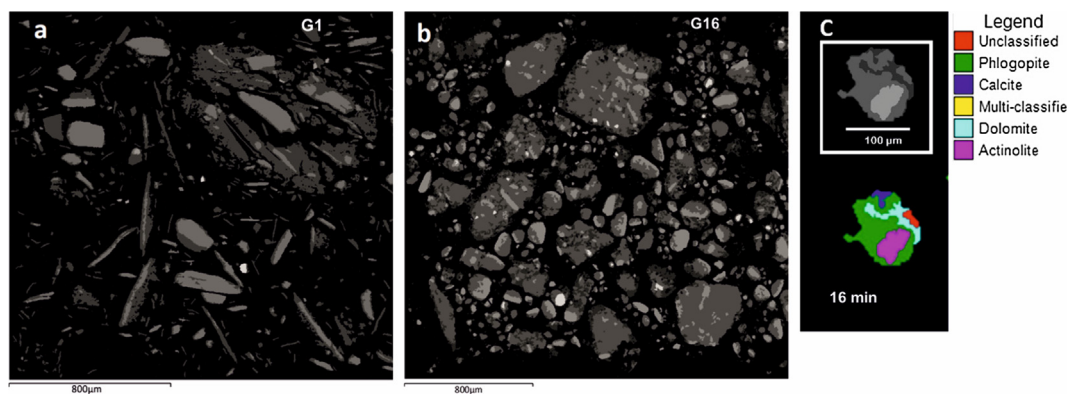
Fig. 10. BSE images for (a) G1, (b) G16 and (c) Chemical analysis of one particle of G16 through MLA.
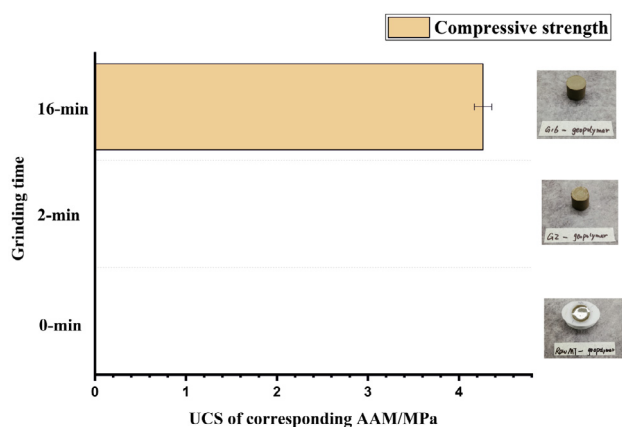

Fig. 11. Unconfined compressive strength of corresponding alkali-activated materials produced by mechanochemically activated mine tailings.

substantiated the improved reactivity of mining wastes presented the feature of amorphous X-ray structure, altered minerology, enhanced alkaline reactivity and larger specific surface area. It also addressed the significance of in-depth understanding of the precursor designed for alkali activation purpose. Mineral liberation analysis was carried out to evaluate the interaction among individual minerals within the precursor. Additionally, structural alternation pathway of phlogopite under intensive grinding was proposed based on the experimental observations. Full structural collapse in not achieved, for example phlogopite tetrahedral layers seem to retain their structure despite of the wholesale structural changes in the interlayer and dehydroxylation within phlogopite octahedral layers. Consequently, mechanically activated phosphate mine tailings revealed inhomogeneous mineral distribution and amorphous phases in individual particles after 16-min grinding, indicating mechanochemical activation through vibratory disc mill can be a promising method to increase the potential of phosphate mine tailings in producing alkali activation materials.

CRediT authorship contribution statement

He Niu: Investigation, Methodology, Writing - original draft. **Paivo Kinnunen:** Conceptualization, Funding acquisition, Supervision, Writing – review & editing. **Harisankar Sreenivasan:** Methodology, Writing – review & editing. **Elijah Adesanya:** Methodology, Writing – review & editing. **Mirja Illikainen:** Conceptualization, Funding acquisition, Supervision, Writing – review & editing.

Declaration of Competing Interest

The authors declare that they have no known competing financial interests or personal relationships that could have appeared to influence the work reported in this paper.

References

Aglietti, E., Lopez, J.P., Pereira, E., 1986. Mechanochemical effects in kaolinite grinding. I. Textural and physicochemical aspects. Int. J. Miner. Process. 16, 125–133.

Aïtcin, P.-C., 2000. Cements of yesterday and today: Concrete of tomorrow. Cem. Concr. Res. 30, 1349–1359. https://doi.org/10.1016/S0008-8846(00)00365-3.

Ávila, P.F., da Silva, E.F., Salgueiro, A.R., Farinha, J.A., 2008. Geochemistry and Mineralogy of Mill Tailings Impoundments from the Panasqueira Mine (Portugal): Implications for the Surrounding Environment. Mine Water Environ. 27, 210–224. https://doi.org/10.1007/s10230-008-0046-4.

Bigham, J.M., Bhatti, T.M., Vuorinen, A., Tuovinen, O.H., 2001. Dissolution and structural alteration of phlogopite mediated by proton attack and bacterial oxidation of ferrous iron. Hydrometallurgy 59, 301–309. https://doi.org/10.1016/S0304-386X (00)00186-9.

Bloise, A., Catalano, M., Gualtieri, A.F., 2018a. Effect of grinding on Chrysotile, Amosite and Crocidolite and implications for thermal treatment. Minerals 8, 135.

Bloise, A., Kusiorowski, R., Gualtieri, A., 2018b. The effect of grinding on tremolite asbestos and anthophyllite asbestos. Minerals 8, 274.

Bradley, W.F., Burst, J., Graf, D.L., 1953. Crystal chemistry and differential thermal effects of dolomite. Rep. Investig. No 167.

Burns, J.H., Bredig, M.A., 1956. Transformation of calcite to aragonite by grinding. 1281–1281. J. Chem. Phys. 25. https://doi.org/10.1063/1.1743198.

Cheng, T.W., Chiu, J.P., 2003. Fire-resistant geopolymer produced by granulated blast furnace slag. Miner. Eng. 16, 205–210. https://doi.org/10.1016/S0892-6875(03) 00008-6.

Choi, S.C., Lee, W.K., 2012. Effect of Fe2O3 on the physical property of geopolymer paste. Adv. Mater. Res. 586, 126–129. https://doi.org/10.4028/www.scientific.net/AMR. 586.126.

Criado, J., Trillo, J., 1975. Effects of mechanical grinding on the texture and structure of calcium carbonate. J. Chem. Soc. Faraday Trans. 1 Phys Chem. Condens. Phases 71, 961–966.

Douglas, E., Bilodeau, A., Brandstetr, J., Malhotra, V.M., 1991. Alkali activated ground granulated blast-furnace slag concrete: Preliminary investigation. Cem. Concr. Res. 21, 101–108. https://doi.org/10.1016/0008-8846(91)90036-H.

Duxson, P., Provis, J.L., Lukey, G.C., van Deventer, J.S.J., 2007. The role of inorganic polymer technology in the development of 'green concrete'. Cem. Concr. Res. 37, 1590–1597. https://doi.org/10.1016/j.cemconres.2007.08.018.

Fandrich, R., Gu, Y., Burrows, D., Moeller, K., 2007. Modern SEM-based mineral liberation analysis. Int. J. Miner. Process. 84, 310–320. https://doi.org/10.1016/j.minpro. 2006.07.018.

Fernando, P.-T., João, C.-G., Said, J., 2010. Durability and environmental performance of alkali-activated tungsten mine waste mud mortars. J. Mater. Civ. Eng. 22, 897–904.

Földvári, M., 2011. Handbook of thermogravimetric system of minerals and its use in geological practice, Occasional papers of the Geological Institute of Hungary.

Geological Inst. of Hungary, Budapest.

Gavish, E., Friedman, G.M., 1973. Quantitative analysis of calcite and Mg-calcite by X-ray diffraction: effect of grinding on peak height and peak area. Sedimentology 20, 437–444.

Giannopoulou, I., Panias, D., 2006. Development of geopolymeric materials from industrial solid wastes. Presented at the 2nd International conference on advances in mineral resources management and environmental geotechnology, Greece.

Hasanbeigi, A., Menke, C., Price, L., 2010. The CO_2 abatement cost curve for the Thailand cement industry. J. Clean. Prod. 18, 1509–1518. https://doi.org/10.1016/j.jclepro.2010.06.005.

Heller-Kallai, L., 1980. Dehydroxylation of Dioctahedral Phyllosilicates. Clays Clay Miner. 28, 355–368. https://doi.org/10.1346/CCMN.1980.0280505.

Jiao, X., Zhang, Y., Chen, T., 2013. Thermal stability of a silica-rich vanadium tailing based geopolymer. Constr. Build. Mater., 25th Anniversary Session for ACI 228 – Building on the Past for the Future of NDT of Concrete 38, 43–47. https://doi.org/10.1016/j.conbuildmat.2012.06.076.

Kalinkina, E., Gurevich, B., Kalinkin, A., 2018. Alkali-Activated Binder Based on Milled Antigorite. Minerals 8, 503. https://doi.org/10.3390/min8110503.

Kinnunen, P., Ismailov, A., Solismaa, S., Sreenivasan, H., Räisänen, M.-L., Levänen, E., Illikainen, M., 2018. Recycling mine tailings in chemically bonded ceramics – A review. J. Clean. Prod. 174, 634–649. https://doi.org/10.1016/j.jclepro.2017.10.280.

Kiventerä, J., Golek, L., Yliniemi, J., Ferreira, V., Deja, J., Illikainen, M., 2016. Utilization of sulphidic tailings from gold mine as a raw material in geopolymerization. Int. J. Miner. Process. 149, 104–110. https://doi.org/10.1016/j.minpro.2016.02.012.

Kristof, E., Juhasz, A., 1993. The effect of intensive grinding on the crystal structure of dolomite. Powder Technol. 75, 145–152.

Kristóf-Makó, É., Juhász, A.Z., 1999. The effect of mechanical treatment on the crystal structure and thermal decomposition of dolomite. Thermochim. Acta 342, 105–114. https://doi.org/10.1016/S0040-6031(99)00290-7.

Kumar, S., Kumar, R., Alex, T.C., Bandopadhyay, A., Mehrotra, S.P., 2007. Influence of reactivity of fly ash on geopolymerisation. Adv. Appl. Ceram. 106, 120–127. https://doi.org/10.1179/174367607X159293.

Liao, J., Senna, M., 1992. Thermal behavior of mechanically amorphized talc. Thermochim. Acta 197, 295–306.

MacKenzie, K.J., Komphanchai, S., Vagana, R., 2008. Formation of inorganic polymers (geopolymers) from 2: 1 layer lattice aluminosilicates. J. Eur. Ceram. Soc. 28, 177–181.

Marjanović, N., Komljenović, M., Baščarević, Z., Nikolić, V., 2014. Improving reactivity of fly ash and properties of ensuing geopolymers through mechanical activation. Constr. Build. Mater. 57, 151–162. https://doi.org/10.1016/j.conbuildmat.2014.01.095.

Martinelli, G., Plescia, P., 2004. Mechanochemical dissociation of calcium carbonate: laboratory data and relation to natural emissions of CO_2. Phys. Earth Planet. Inter. 142, 205–214.

Moukannaa, S., Loutou, M., Benzaazoua, M., Vitola, L., Alami, J., Hakkou, R., 2018. Recycling of phosphate mine tailings for the production of geopolymers. J. Clean. Prod. 185, 891–903.

Nefedov, V.I., 1988. X-ray photoelectron spectroscopy of solid surfaces. Springer Science & Business.

Ozcan, O., Benzer, H., 2013. Comparison of different breakage mechanisms in terms of product particle size distribution and mineral liberation. Miner. Eng. 49, 103–108. https://doi.org/10.1016/j.mineng.2013.05.006.

Pacheco-Torgal, F., Castro-Gomes, J., Jalali, S., 2009. Tungsten mine waste geopolymeric binder: preliminary hydration products investigations. Constr. Build. Mater. 23, 200–209.

Phair, J.W., van Deventer, J.S.J., 2002. Characterization of fly ash-based geopolymeric binders activated with sodium aluminate. Ind. Eng. Chem. Res. 41, 4242–4251. https://doi.org/10.1021/ie010937o.

Plescia, P., Gizzi, D., Benedetti, S., Camilucci, L., Fanizza, C., De Simone, P., Paglietti, F., 2003. Mechanochemical treatment to recycling asbestos-containing waste. Waste Manag. 23, 209–218.

Provis, J., 2014a. Alkali Activated Materials, 1st ed. RILEM State-of-the-Art Reports. Springer, Netherlands.

Provis, J.L., 2014b. Geopolymers and other alkali activated materials: why, how, and what? Mater. Struct. 47, 11–25. https://doi.org/10.1617/s11527-013-0211-5.

Rayner, J.H., 1974. The crystal structure of phlogopite by neutron diffraction. Miner. Mag. 39, 850–856.

Sanchez-Soto, P., Justo, A., Perez-Rodriguez, J., 1994. Grinding effect on kaolinite-pyrophyllite-illite natural mixtures and its influence on mullite formation. J. Mater. Sci. 29, 1276–1283.

Sarker, P.K., Kelly, S., Yao, Z., 2014. Effect of fire exposure on cracking, spalling and residual strength of fly ash geopolymer concrete. Mater. Des. 63, 584–592.

Siegbahn, K., Nordling, C., 1967. ESCA, atomic, molecular and solid state structure studied by means of electron spectroscopy. Nov Act Uppsaliensis.

Silva, I., Castro-Gomes, J.P., Albuquerque, A., 2012. Effect of immersion in water partially alkali-activated materials obtained of tungsten mine waste mud. Constr. Build. Mater. 35, 117–124.

Song, M., Jiaping, L., Qian, J., Jianzhong, L., Liang, S., 2016. Experimental study on utilization of quartz mill tailings as a filler to prepare geopolymer. Miner. Process. Extr. Metall. Rev. 37, 311–322.

Sreenivasan, H., Kinnunen, P., Heikkinen, E.-P., Illikainen, M., 2017. Thermally treated phlogopite as magnesium-rich precursor for alkali activation purpose. Miner. Eng. 113, 47–54.

Sutherland, D.N., Gottlieb, P., 1991. Application of automated quantitative mineralogy in mineral processing. Miner. Eng. 4, 753–762. https://doi.org/10.1016/0892-6875(91)90063-2.

Temuujin, J., Williams, R.P., Van Riessen, A., 2009. Effect of mechanical activation of fly ash on the properties of geopolymer cured at ambient temperature. J. Mater. Process. Technol. 209, 5276–5280.

Terashima, W., Che, S.-B., Ishitani, Y., Yoshikawa, A., 2006. Growth and characterization of AlInN ternary alloys in whole composition range and fabrication of InN/AlInN multiple quantum wells by RF molecular beam epitaxy. Jpn. J. Appl. Phys. 45, L539.

Turner, L.K., Collins, F.G., 2013. Carbon dioxide equivalent (CO_2-e) emissions: A comparison between geopolymer and OPC cement concrete. Constr. Build. Mater. 43, 125–130.

Tutti, F., Dubrovinsky, L.S., Nygren, M., 2000. High-temperature study and thermal expansion of phlogopite. Phys. Chem. Miner. 27, 599–603. https://doi.org/10.1007/s002690000098.

Udagawa, S., Urabe, K., Hasu, H., 1974. The crystal structure of muscovite dehydroxylate. J. Jpn. Assoc. Mineral. Petrol. Econ. Geol. 69, 381–389.

Van, J., Lukey, G.C., Van, D., Graham, A., 2000. The stabilisation of mine tailings by reactive geopolymerisation. Presented Australasian Inst Min Metall Publ Ser 363–372.

Vatopoulos, K., Tzimas, E., 2012. Assessment of CO_2 capture technologies in cement manufacturing process. J. Clean. Prod. 32, 251–261. https://doi.org/10.1016/j.jclepro.2012.03.013.

Vickers, L., van Riessen, A., Rickard, W.D.A., 2015. Fire-resistant geopolymers, springerbriefs in materials. Springer Singapore, Singapore https://doi.org/10.1007/978-981-287-311-8.

Vizcarra, T.G., Wightman, E.M., Johnson, N.W., Manlapig, E.V., 2010. The effect of breakage mechanism on the mineral liberation properties of sulphide ores. Miner. Eng. 23, 374–382. https://doi.org/10.1016/j.mineng.2009.11.012.

Wardle, R., Brindley, G., 1972. The crystal structures of pyrophyllite, 1Te, and of its dehydroxylate. Am. Mineral. J. Earth Planet. Mater. 57, 732–750.

WARNE, S.S.J., 1977. Carbonate mineral detection by variable atmosphere differential thermal analysis. 678–678. Nature 269. https://doi.org/10.1038/269678a0.

Wei, B., Zhang, Y., Bao, S., 2017. Preparation of geopolymers from vanadium tailings by mechanical activation. Constr. Build. Mater. 145, 236–242 https://doi.org/10.101/j.conbuildmat.2017.03.234.

Xiao, X., Zhang, G., Feng, Q., Xiao, S., Huang, L., Zhao, X., Li, Z., 2012. The liberation effect of magnetite fine ground by vertical stirred mill and ball mill. Miner. Eng. 34, 63–69. https://doi.org/10.1016/j.mineng.2012.04.004.

Xu, H., Van Deventer, J.S.J., 2000. The geopolymerization of alumino-silicate minerals. Int. J. Miner. Process. 59, 247–266. https://doi.org/10.1016/S0301-7516(99)00074-5.

Ye, J., Zhang, W., Shi, D., 2014. Effect of elevated temperature on the properties of geopolymer synthesized from calcined ore-dressing tailing of bauxite and ground-granulated blast furnace slag. Constr. Build. Mater. 69, 41–48.

Ye, N., Chen, Y., Yang, J., Liang, S., Hu, Y., Xiao, B., Huang, Q., Shi, Y., Hu, J., Wu, X., 2016. Co-disposal of MSWI fly ash and Bayer red mud using an one-part geopolymeric system. J. Hazard. Mater. 318, 70–78. https://doi.org/10.1016/j.jhazmat.2016.06.042.